ChemSystemsChem

Research Article
doi.org/10.1002/syst.202400061

Chemistry Europe
European Chemical Societies Publishing

www.chemsystemschem.org

VIP *Very Important Paper*

Non-Uniform Electric Field Manipulation of Chromogenic Peptide Amphiphile Assemblies

Kiara L. Lacy[+],[a] Sujeung Lim[+],[a] Emil M. Lundqvist,[b] Yuyao Kuang,[a] Harrison C. Jeong,[a] Tayloria N. G. Adams,*[a, b, c] and Herdeline Ann M. Ardoña*[a, b, c, d]

Herdeline Ann M. Ardoña has been nominated for the special collection Systems Chemistry Talents by Board Members Dave Adams and Rein Ulijn.

This work investigates the influence of dielectrophoretic forces on the structural features and the resulting aggregates of a chromogenic model system, peptide-diacetylene (D_3GV-DA) amphiphiles. Here, we systematically investigate how non-uniform electric fields impact the (i) peptide-directed supramolecular assembly stage and (ii) topochemical photopolymerization stage of polydiacetylenes (PDAs) in a quadrupole-based dielectrophoresis (DEP) device, as well as the (iii) manipulation of D_3GV-DA aggregates in a light-induced DEP (LiDEP) platform. The conformation-dependent chromatic phases of peptide-PDAs are utilized to probe the chain-level effect of DEP exposure after the supramolecular assembly or after the topochemical photopolymerization stage. Steady-state spectroscopic and microscopy analyses show that structural features such as the chirality and morphologies of peptidic 1-D nanostructures are mostly conserved upon DEP exposure, but applying mild, non-uniform fields at the self-assembly stage is sufficient for fine-tuning the chromatic phase ratio in peptide-PDAs and manipulating their aggregates via LiDEP. Overall, this work provides insights into how non-uniform electric fields offer a controllable approach to fine-tune or preserve the molecularly preset assembly order of DEP-responsive supramolecular or biopolymeric assemblies, as well as manipulate their aggregates using light projections, which have future implications for the precision fabrication of macromolecular systems with hierarchical structure-dependent function.

Introduction

External physical factors that complement synthetic design tools for controlling the multi-scale organization of macromolecular building blocks pave the way for achieving new or improved physicochemical properties for functional organic materials. Triggering or controlling the formation of macromolecular structures has often been reported via direct alteration of the solution formulation or distortion of the system structure through pH,[1,2] temperature,[3,4] or mechanical force[5] changes. On the other hand, indirect contact approaches for influencing macromolecular structure, such as the utility of light[6,7] or electromagnetic fields,[8,9] offer the advantage of milder conditions for remotely manipulating the organization of monomeric building blocks or the resulting polymer. More specifically, these fields have been shown to tune reaction kinetics and side chain interactions by controlling the orientation and direction of assembling molecules in a supramolecular assembly.[9,10] For example, the use of an external electric field on the piezoelectric diphenylalanine (FF) was reported to cause stretching of the FF peptide backbone and increase the rate of aggregation within the system, which gives insight into the influence of electric fields to control aggregate formation of piezoelectric peptides to better understand their electromechanical properties.[11] Electric field modulation has been used to influence the alignment or 2-D framework of supramolecular assemblies. Cometto et al. used external electric fields to control the switching of hydrogen-bonded networks and found that intermolecular and molecular-surface interactions influence the switching, rather than just the properties of individual molecules.[12] In other cases, non-uniform electric fields have been used to manipulate nanoparticles,[13] block co-polymers,[14] and supramolecular fibers[9] within fluids.

Here, we investigate the usage of dielectrophoresis (DEP), an electrokinetic technique that utilizes a non-uniform electric field, to manipulate an amphiphilic and chromogenic peptide-polymer conjugate as a model system. DEP is known to offer real-time characterization and nano-to-micron-range particle

[a] *Department of Chemical and Biomolecular Engineering, Samueli School of Engineering, University of California, Irvine, CA, United States*
[b] *Department of Biomedical Engineering, Samueli School of Engineering, University of California, Irvine, CA, United States*
[c] *Sue & Bill Gross Stem Cell Research Center, University of California, Irvine, CA, United States*
[d] *Department of Chemistry, School of Physical Sciences, University of California, Irvine, CA, United States*

Correspondence: *Tayloria N. G. Adams and Herdeline Ann M. Ardoña, Department of Chemical and Biomolecular Engineering, Samueli School of Engineering, University of California, Irvine, CA 92697, United States.*
Email: tayloria@uci.edu and hardona@uci.edu

[+] *These authors contributed equally to the manuscript.*

Supporting information for this article is available on the WWW under https://doi.org/10.1002/syst.202400061

manipulation by often utilizing an alternating current (AC) electric field to polarize particles and induce movement based on the frequency of the applied voltage.[15] The frequency of the electric field controls the response of the particle, in which it can be attracted or repelled from the electrodes, referred to as positive and negative DEP, respectively (Figure 1a). Traditional DEP methods incorporate physical metal electrodes to create a non-uniform electric field. Other DEP modalities also exist, such as light-induced DEP (LiDEP) that uses light projections, referred to as "virtual electrodes", to generate a non-uniform electric field (Figure 1b). These DEP methods induce particle movement and offer a pathway for pattern-specific manipulation of particles. In a broad context, DEP has been used in applications, such as the characterization and manipulation of proteins,[16,17] human mesenchymal stem cells (hMSCs),[18–20] and DNA.[21,22] To investigate the influence of DEP forces in this study, polydiacetylene (PDA) was specifically selected as the polymeric model due to its known stimuli-responsive chromogenicity.[23–28] PDAs are formed through the polymerization of ordered diacetylene (DA) monomers with ultraviolet (UV) light irradiation, to form a conjugated ene-yne backbone (Figure 1c).[29] Upon exposure to external stimuli, the measurable chromatic transitions are mainly attributed to chain conformation changes of PDAs from a planar, non-fluorescent, blue phase (λ_{max}~640 nm) to a non-planar, fluorescent, red phase (λ_{max}~520 nm) (Figure 1d).[30] These conformation-dependent chromatic transitions that can be easily monitored via spectroscopic techniques make PDAs ideal as a model system for elucidating the impact of external stimuli on the order of a macromolecular assembly system.

In this work, we specifically investigate the effect of non-uniform electric field stimulation at multiple structural length scales for DA units conjugated to a pentapeptide, triaspartic-glycine-valine (DDDGV, denoted as D_3GV).[24] The amphiphilic diacetylene monomer design utilized in our study bears a charged peptidic moiety as the polar group that provides a supramolecular template for the geometric requirements of PDA topochemical polymerization to be satisfied, as well as a synthetic handle to control its stimuli-responsive properties, as shown in our previous reports.[24,31,32] With DEP as a stimuli, we sought to investigate how non-uniform AC fields can interact with charged peptide-diacetylene systems via manipulation of its supramolecular and topochemically polymerized aggregates. Using a suite of spectroscopic measurements and microscopy, we characterized the influence of DEP force on the structural features of peptide-DA/-PDA during the (i) peptide-directed supramolecular aggregation stage, (ii) topochemical photo-polymerization stage, as well as the (iii) manipulation of D_3GV-DA aggregates in a light-induced DEP platform. We investigated the use of LiDEP to induce peptide-DA aggregate movement and explored this technique for manipulation of PDA precursors at its supramolecular assembly stage. Within the scope of this paper, we demonstrate the potential of DEP-based approaches to manipulate peptide-PDA aggregates and systematically identify the conditions by which structural features of the 1-D assemblies are conserved or fine-tuned.

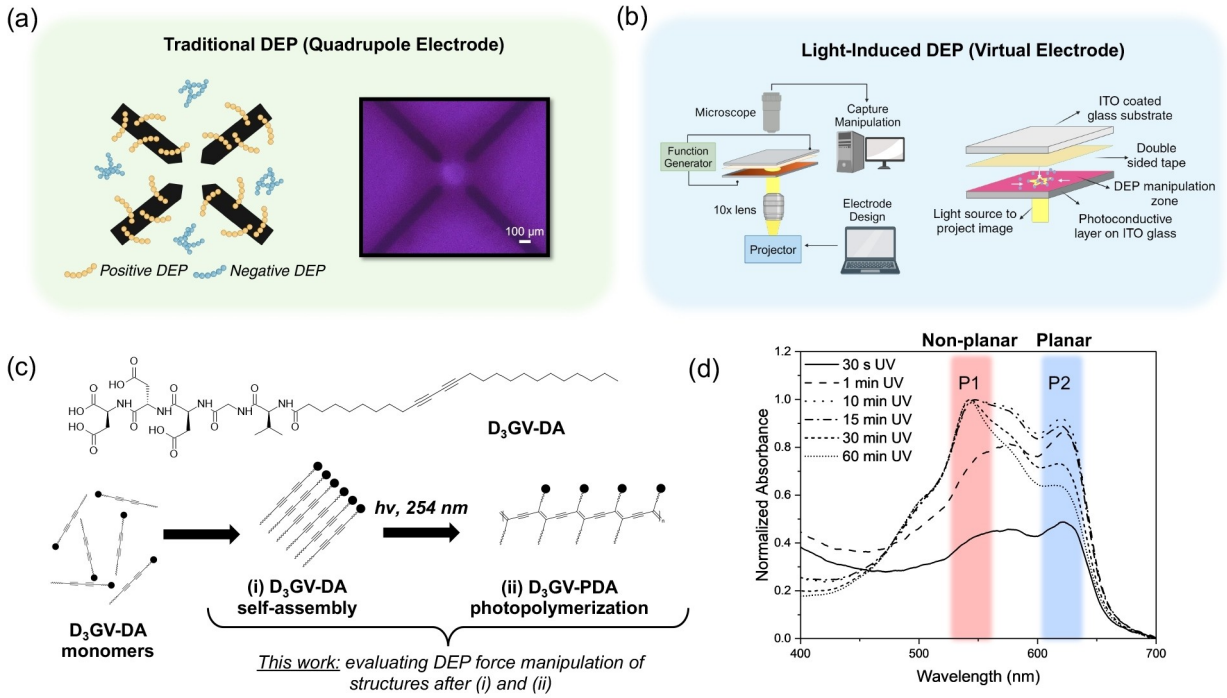

Figure 1. General schematic for the DEP device platforms used and for the formation of peptide-polydiacetylene conjugates. (a) DEP is used as a stimuli to manipulate D_3GV-DA/-PDA assemblies using a quadrupole device. (b) LiDEP is also introduced as a method to manipulate supramolecular peptide-DA nanostructures. (c) Schematic illustration of the self-assembly of peptide-diacetylene monomers that form peptide-PDAs after UV light irradiation. (d) As self-assembled peptide-DAs polymerize under UV irradiation, the non-fluorescent blue-phase polymer (P2; λ_{max}~620 nm) is formed. Upon further UV stimulation, the PDA backbone twists, and the intensity of the peak corresponding to the non-planar, red fluorescent polymer (P1; λ_{max}~540 nm) increases. Figure 1a and b were made in part using BioRender.

Materials and Methods

General Terms and Considerations

Fmoc-protected amino acids and Wang resin were acquired from Advanced ChemTech. 10,12-pentacosadiynoic acid and formic acid were purchased from Sigma-Aldrich. Acetonitrile (ACN), *O*-(benzotriazole-1-yl)-*N,N,N′,N′*-tetramethyluronium hexafluorophosphate (HBTU), benzoatriazol-1-yl-oxy-tripyrrolidinophosphonium hexafluorophosphate (PyBOP), trifluoroacetic acid (TFA), triisopropylsilane (TIPS), *N*-*N*-diisopropylethylamine (DIPEA), *N*-methylpyrrolidinone (NMP), methanol, dichloromethane (DCM), dimethylformamide (DMF), ammonium hydroxide, were obtained from Oakwood Products, Inc. or Fisher Scientific. UltraPure™ DNase/RNase-Free Distilled Water was obtained from Thermo Fisher Scientific. Amorphous silicon (a:Si) targets were purchased from Millipore Sigma. Molybdenum targets were obtained from Kurt J. Lesker Company. Indium tin oxide glass slides were obtained from MSE Supplies LLC. Copper tape was obtained from Zehhe. A stock solution of Tween-20 (2.24 wt%) was purchased from Chem-Impex International, Inc.

Synthesis, Purification and Characterizations of Peptide-Diacetylene Monomer

The peptide-diacetylene monomer (D_3GV-DA) was synthesized and purified as previously reported in the literature.[24] The mass and the structure of the D_3GV-DA were consistent with the previously reported electrospray ionization mass spectrometry (ESI-MS) and nuclear magnetic resonance (NMR) spectroscopy data (Figures S1 and S2).[24]

Fabrication of Quadrupole Electrodes

Electrodes with quadrupole geometry were fabricated using a Heidelberg MLA150 Laser Writer, consisting of a 50 μm layer of titanium as an adhesive layer and 50 μm of gold on a glass substrate. The electrode width was 100 μm with a 200 μm spacing at the tip of the electrodes. Polydimethylsiloxane (PDMS) with a 6 mm diameter hole was plasma bonded to the glass substrate centered on the device, creating the region of sample manipulation.

Sample Preparation

D_3GV-DA (theoretical isoelectric point, pI, 2.78) samples were prepared using a 1 mM acetate buffer to a final concentration of 2.3 mM. A 1 mM acetate buffer was made by diluting a stock solution of 0.1 M solution with sodium acetate and acetic acid in UltraPure™ DNase/RNase-Free Distilled Water on the day of the experiment. The pH and conductivity of the buffer were kept around ~5 and ~65 μS/cm, respectively, across all conditions. To form the peptide-PDA samples, a 254 nm UV light source was used to polymerize the self-assembled D_3GV-DA in acetate buffer.

Traditional DEP Modulation of D_3GV-PDA

A description of dielectrophoretic considerations for the device platform used here is described in the Supporting Information. AC electric field modulation during the polymerization process was investigated with the quadrupole-based DEP device (Figure S3) by observing the non-covalent peptide-directed assemblies of supramolecular aggregates of D_3GV-DA and UV-irradiation-assisted covalent polymerization to form PDAs. The condition where non-covalent peptide-directed assemblies were exposed to AC electric field prior to UV-polymerization is denoted as **"DEP + UV"**. Samples were placed into the PDMS well and exposed to a DEP field with the desired set frequency (kHz) and peak-to-peak voltage (V_{pp}) ranging from 10 V_{pp} to 20 V_{pp}, using a function generator (Tektronix AFG 31000), then polymerized with a UV light source. Electrical stimulation was continued throughout the UV-irradiation process. To observe the influence of AC electric field on D_3GV-PDA, exposure to DEP was done after the sample was exposed to a UV light within the PDMS well and exposed to the DEP field for the same time ranges, denoted as **"UV + DEP"**. Between each sample run, the well was washed with Milli-Q water, wiped with a cotton swab containing 70% ethanol, and washed again 3 times with Milli-Q water to remove any leftover samples.

LiDEP Manipulation

The experimental setup of the LiDEP platform includes a projector (Vecupou), a digital microscope (Keyence VHX-7000), a function generator (Tektronix AFG 31000), a LiDEP chip, and a laptop. The virtual electrodes were generated via Microsoft PowerPoint (or an analogous graphic-building software), which were then projected onto the chip through a 10x objective lens. The LiDEP chip consists of three layers: (1) a bottom photoconductive layer deposited onto an indium tin oxide (ITO) glass substrate; (2) a microchannel layer cut out from double-sided tape; and (3) a top ITO glass substrate with holes drilled for the inlet and outlet to introduce the sample solution. The copper tape was connected to the top and bottom ITO glass slides to create the electric circuit. The device material was made of 10 nm layer of molybdenum to smooth out the ITO surface and act as an adhesive layer, and 1 μm photoconductive layer of amorphous silicon. Figure 1b illustrates the LiDEP setup. When illuminated, the conductivity in the light-illuminated area increases and generates a virtual electrode. When the AC electric field was applied, the material of interest (self-assembled peptide-DAs or peptide-PDA) experienced positive or negative DEP response with respect to the electrode. Yellow (hex code #FFFF00) was chosen as the input color of the virtual electrode projected onto the device, based on our previous work with LiDEP.[19] Samples for LiDEP manipulation were prepared in the same way as the samples for quadrupole

devices, such that the D_3GV-DA material was placed into the LiDEP device at 2.3 mM in the 1 mM acetate buffer solution before the light and AC field was applied. Due to the small volume of media in the device, as well as light stimulation of the material, experimental run times were kept below five minutes to prevent channel drying and unwanted light polymerization of the sample. The light is turned on prior to applying the electric field so that the DA aggregate movement can be more visibly observed.

Ultraviolet-Visible (UV-Vis) Absorption Spectroscopy

UV-Vis absorption spectra of the D_3GV-PDA were obtained using a Cary 100 UV-Vis spectrophotometer. The same samples that went through the AC electric field stimulation were diluted with UltraPure™ DNase/RNase-Free Distilled Water at a final concentration of 0.31 mM. The acidic buffer concentration was 0.13 mM. All spectra were normalized with the signals from the self-assembled samples (no UV) control subtracted out.

Atomic Force Microscopy (AFM)

Atomic force microscopy (AFM) images were taken using the tapping mode of a Tosca™ 400 AFM (Anton Paar, Graz, Austria). The optimum amplitude of the cantilever and laser alignment were calibrated automatically using the Tosca™ Control software. Images were taken at a resolution of 300×300 px, and a line speed of 2.0 lines/sec or 1.0 lines/sec for 5×5 μm and 1×1 μm images respectively. AFM images were taken at multiple locations for each sample to account for any heterogeneities in nanostructure density as a consequence of the dropcasting procedure at a concentration of 0.31 mM. Images were then processed using Gwyddion software (Czech Metrology Institute, Czechia).

Transmission Electron Microscopy (TEM)

Samples were deposited on formvar coated (10 nm) copper grids in 200 mesh with a carbon coating (1 nm) (Electron Microscopy Services). Grids were prepared by briefly dipping them in 1 wt% Tween-20 in UltraPure™ DNase/RNase-Free Distilled Water and blotting the excess solution with filter paper. To deposit samples onto grids, 5 μL of a sample was deposited onto the carbon face of the grid for 1 minute. Following the coating, grids were dried from the copper face and sides. Images were taken with the JEOL JEM-2100F at UC Irvine Materials Research Institute and processed using Gatan Digital Micrograph. The lengths of 1-D nanostructures in each condition were analyzed using Nano Measurer.

Hyperspectral Microscopy

A hyperspectral microscope with CytoViva Enhanced Darkfield Illuminator was used. After applying the UV/DEP exposure to peptide-PDA samples, the solutions were mounted onto a clear microscope glass slide to be visualized. Brightfield images were taken at 50× and 100× to observe the assemblies of the peptidic materials. ENVI version 4.8 (Exelis Visual Information Solutions, Boulder, Colorado) was used for data analysis to develop the Spectral Angle Mapping (SAM) images. Image processing was done using Fiji.[33]

Circular Dichroism (CD) Spectroscopy

CD spectra were obtained using a Jasco J-810 spectropolarimeter. The same samples used for UV-vis spectroscopy were utilized to obtain the spectra for the peptide-PDA samples in the visible light region (300–700 nm). Then, the same samples were diluted to 0.063 mM using UltraPure™ DNase/RNase-Free Distilled Water to obtain the spectra for the peptide region (190–260 nm).

RGB Analysis

Images of each condition were taken on a Keyence BZ–X800. Images were split into respective red, green, and blue color channels and intensities were quantified using Fiji.[33] The average intensity is plotted, and the error bars represent the standard deviation.

Results and Discussion

In this study, D_3GV-DA/-PDA was used as a model system to study the influence of DEP on a chromogenic macromolecular assembly system. Our peptide-DA monomer was carefully designed to contain ionizable amino acids, aspartic acid (D), at the C-termini of the peptide sequence to promote solubility in water and generate aggregates with charged side chains. Glycine (G) was incorporated in the peptide sequence to serve as a spacer after the triaspartic acid residues and valine (V) were chosen based on its high propensity to form a β-sheet as a secondary structure. In our previous work, the D_3GV peptide moiety served as an effective template for the amphiphilic DA monomers to satisfy the geometric requirements for the topochemical polymerization towards D_3GV-PDA formation, as well as a synthetic handle for modulating the thermochromicity of PDAs when coassembled with its charge-complementary pair under neutral conditions.[24,32] Here, the charged D_3GV-DA/-PDA samples were prepared in a buffered solution at a pH of ~5 (*i.e.*, above the theoretical pI of the peptide region, 2.78), with a conductivity of ~65 μS/cm. Under the conditions used for this study, the population of red-phase, non-planar chains predominates over the blue-phase chains as the UV exposure time increases during polymerization (Figure 1d).

For the samples used for DEP experiments, we chose a UV polymerization time of 10 minutes due to the similar apparent coexistence ratio of the planar and non-planar D_3GV-PDA components (~1 : 1 red-to-blue phase ratio or P1/P2; Figure 1d) and to allow for a standardized comparison across conditions during the DEP manipulation experiments (Figure 2; Figure S4–S6). For the device conditions, we mainly applied 10 kHz and a voltage range of 10 V_{pp} to 20 V_{pp} of AC field to the quadrupole device. These conditions induced a positive DEP response for peptide-DAs/-PDAs, as shown by the accumulation of materials around the electrode after 30 minutes of DEP exposure (Figure 2a; representation of the electric field gradient in the quadrupole device can be seen in Figure S3). To first assess how different frequencies can affect the behavior of D_3GV-DA, we observed the migration behavior of peptide assemblies in the frequency range of 5 kHz to 1 MHz, which all showed positive DEP responses (Figure S7; Supplementary Videos S1–S4). Typically, biological cells with micron-scale dimensions demonstrate negative DEP responses at 10 kHz.[18,20] However, several factors such as particle charge,[21,34] shape,[15,35] and conductivity of the particle and solution[21,36] can induce positive DEP in this low frequency range due to the nanostructural nature of these materials. The behavior of our ionizable peptidic assemblies presented here is with respect to the nature of those nanostructures formed in acidic, low conductivity aqueous medium under a non-uniform AC field. To systematically assess the influence of DEP forces on our materials, we also investigated the influence of the duration of non-uniform electric field stimulation at 10 kHz and 10 V_{pp} on D_3GV-PDAs post-UV polymerization. The absorbance profiles show that the increased duration of DEP exposure times have minimal effects on the conformation of the π-conjugated backbone within D_3GV-PDA (Figure 2b; Figure S4; Table S1). When DEP strength is altered as a consequence of voltage amplitude between 15 V_{pp} and 20 V_{pp} (Figure 2c; Figure S5b), a relatively higher P1/P2 ratio for peptide-PDA samples was observed (Table S2).

Next, we considered how exposure to DEP forces could influence the supramolecular assembly prior to UV-induced topochemical polymerization. Briefly, DA monomers polymerize into PDAs through a 1,4-addition upon UV-irradiation, which is often supported by DAs with amphiphilic characteristics.[30,37] The normalized absorbance profiles show that DEP exposure (20 V_{pp}) of the monomer assembly resulted in a decrease in the intensity of the blue-phase peaks, suggesting an increase in the presence of non-planar, red-phase PDAs (Figure 2d). On the other hand, the raw absorbance profiles show that the DEP-induced aggregation of monomers to the electrode results in higher intensity of both red- and blue-phase peaks, suggesting a more favored PDA formation (Figures S5 and S6). The self-assembled condition (no UV exposure) was used as a control to

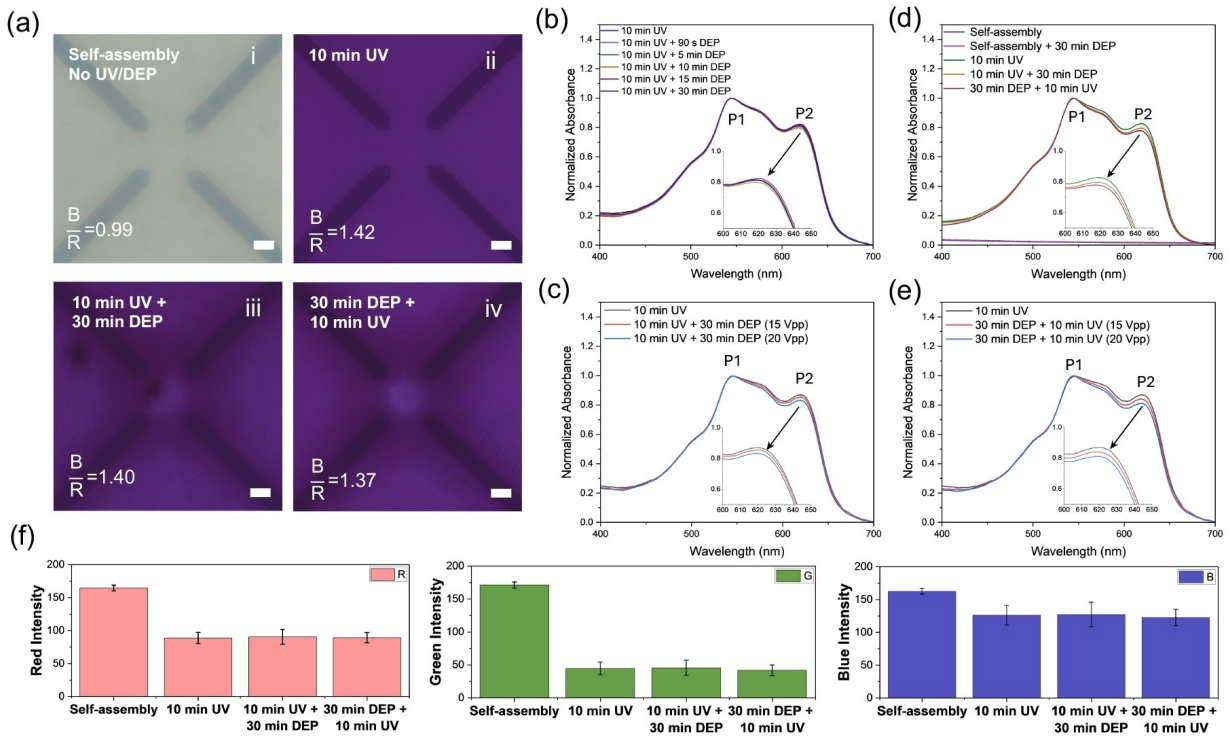

Figure 2. Photophysical characterization of D_3GV-PDA behavior after DEP modulation and UV polymerization. D_3GV-DA/-PDA aggregates are suspended in acetate buffer (pH ~5; ~65 μS/cm). (a) Visualization of peptidic assemblies in the quadrupole device for the (i) self-assembled peptide-DA, (ii) after 10 minutes of UV exposure, (iii) after 10 minutes of UV followed by 30 minutes of DEP exposure, "10 min UV + 30 min DEP", and (iv) 30 minutes of DEP followed by 10 minutes of UV exposure "30 min DEP + 10 min UV" (scale bar: 100 μm). The electric field was supplied at 10 kHz and 20 V_{pp}, unless otherwise noted. Ultraviolet-visible (UV-Vis) absorption spectroscopy was used to measure the absorbance value for each condition. (b) Electrical stimulation post- UV has minimal effects on the blue vs. red phase ratio of PDA, at 10 kHz and 10 V_{pp}. (c) Order of DEP response affects the blue vs. red phase ratio. (d,e) Increasing the electric field both pre- and post- UV increases the P1 (red phase)/P2 (blue phase) ratio. (f) RGB output from quadrupole runs for each condition. The B/R ratio correlates to the values obtained from the relative red and blue intensities.

show that exposure of the material to non-uniform electric fields, under the experimental conditions used, was not causing the sample to polymerize. The observed subtle decrease in blue-phase PDA within the "30 min DEP + 10 min UV" condition could be attributed to a slight disruption of assembly order by applying DEP stimuli during the UV-assisted polymerization, leading to a relative increase in the intensity of the peak reminiscent of a twisted PDA backbone (red-phase). Increasing the voltage amplitude for this sample set also increases the presence of non-planar D_3GV-PDA assemblies (Figure 2e; Figure S5), thus, a higher P1/P2 ratio for peptide-PDA samples was measured (Table S2). To complement the qualitative observation from the spectra shown in Figure 2b–e, we note that the Student's *t*-test analyses for P1/P2 values between the DEP exposed conditions vs. the 10 min UV condition show *p*-values >0.05, confirming the conservation of chain conformation-dependent absorbance for majority of the DEP exposure conditions used here (other than the subtle changes that were most apparent when the order of DEP stimulation was applied prior to UV-assisted photopolymerization; Figure 2d and e). In addition, the RGB analysis of the samples shows that the blue-to-red phase ratio (B/R) decreases under the influence of DEP modulation (Figure 2f). Altogether, these results further validate that the mild, non-uniform DEP fields induced minimal influence on the supramolecular aggregation stage of DA units, while the conformation of PDAs remains generally conserved when experiencing DEP forces.

By examining the circular dichroism (CD) spectra of D_3GV-PDA in the region associated with PDA absorption (300–700 nm), we were able to see that the chiral nature of the chains formed after topochemical photopolymerization is conserved in any of the conditions used. A bisignate signal due to the Cotton effect was observed in this region, which can be attributed to the inherent chirality introduced by the peptides to DA assemblies (Figure 3a). In the region associated with the peptides (190–260 nm), we see a non-traditional, positive CD signature (Figure S8a), potentially due to the scattering effects of aggregates within this region (Figure S8b). To observe any

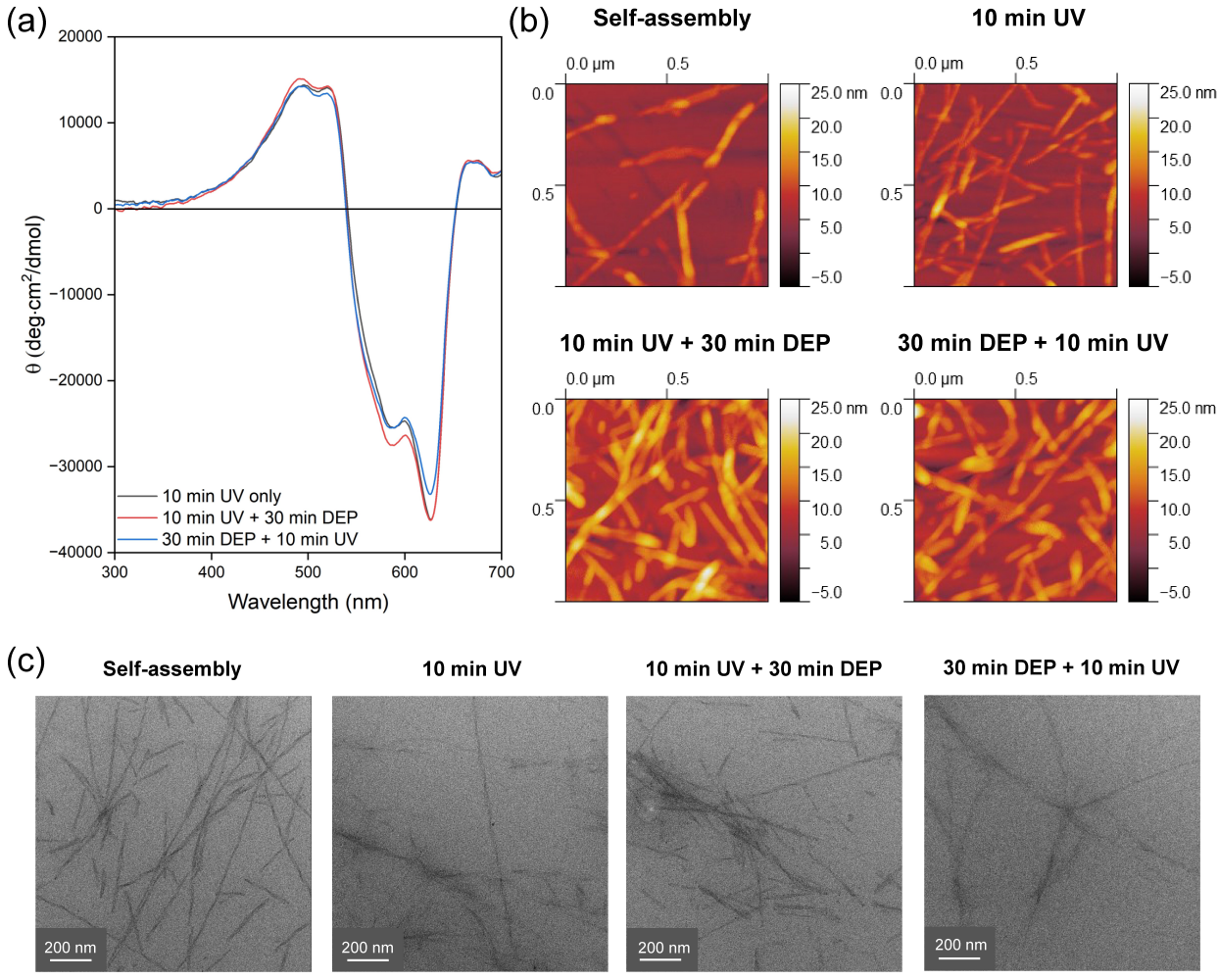

Figure 3. Characterization of the 1-D nanostructure of D_3GV-PDA with or without exposure to DEP forces. (a) CD spectra of the material in the PDA absorption region (300–700 nm). Left-handed chirality of the system is conserved even after exposure to 20 V_{pp} DEP field. (b) AFM images support the consistent formation of 1-D nanostructure of D_3GV-PDA across multiple conditions and compare the influence of DEP field modulation. Materials were dropcasted onto a clear glass slide at 0.31 mM. (c) Representative TEM images from each experimental condition, illustrating the preservation of 1-D nanostructures of D_3GV-DA/-PDA (2.3 mM) across conditions (Scale bar = 200 nm). Length distribution from TEM images of self-assembly: 446.77 ± 136.43 nm; 10 min UV: 381.52 ± 147.11 nm; 10 min UV + 30 min DEP: 391.35 ± 110.29 nm; and 30 min DEP + 10 min UV: 503.11 ± 164.35 nm; mean ± s.e.m.

impacts of DEP forces on the nanostructure morphologies across the samples, AFM was used on D_3GV-DA/-PDA samples with or without DEP field stimulation (Figure 3b; Figure S9). The D_3GV-DA self-assembly and D_3GV-PDA polymerized under UV for 10 minutes were used as control samples to compare the DEP field stimulated conditions, all of which show high aspect ratio 1-D nanostructures. Similarly, the TEM data show consistent nanostructure formation across conditions post-DEP manipulation (Figure 3c). These observations suggest that exposure of the material system here to non-uniform AC electric fields has minimal influence on the nanostructure morphologies. Although the aggregation around quadrupole electrodes is clear across all DEP-exposure conditions, this field-induced crowding of nanostructures seemed unlikely to cause lateral bundling to increase in the height/width of the 1-D nanostructures since the peptide-DAs and -PDAs are charged under the pH used for these experiments. Altogether, these structural characterization data show that the secondary structure/chirality and nanostructure morphologies are conserved regardless of whether the DEP exposure was performed before or after photopolymerization.

To augment the information extracted from the spectroscopic measurements and microscopy, hyperspectral imaging was employed for solutions of peptide-PDA aggregates with or without exposure to DEP forces (Figure 4; Figure S10). SAM analysis of the resulting images enables the visualization of the structural/conformational heterogeneity leading to chromatic phase domains within discrete structures of peptide-PDAs formed across multiple conditions.[38] Two reference spectral profiles (10 min UV sample at pH 5 and 10 min UV sample at pH 10) were specifically selected for the mapping, as the predominant spectra found in 10 min UV sample at pH 5 (local λ_{max}~550, 650 nm; Figure 4b) is reminiscent of peaks for planar, blue-phase of PDA, while the 10 min UV sample at pH 10 is comparable with a twisted, red-phase PDA chains (local λ_{max}~500, 550 nm; Figure 4c). We note that the spectral reference obtained from the 10 min UV sample at pH 5 shows a broader spectral profile than those previously reported for blue-phase PDA[31,38] (hence, we will denote this below as *blue-phase-like PDA domains*), though this deviation is not surprising considering the distinct purple appearance of the aggregates under brightfield. SAM shows that the blue-phase-like domains that predominate in 10 min UV (pH~5) samples continue to be

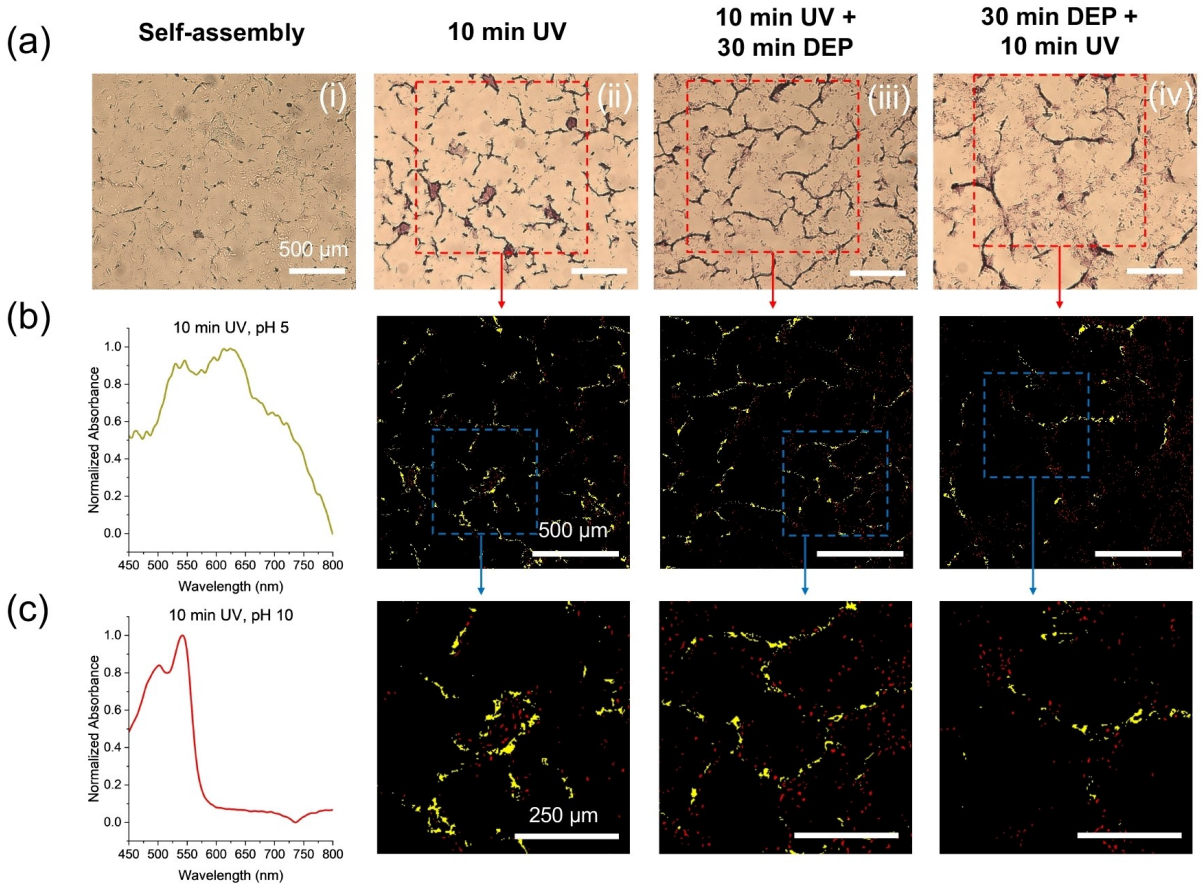

Figure 4. Hyperspectral visualization of conformational heterogeneity in D_3GV-PDA under different UV/DEP exposure conditions. Characterization of the 1-D nanostructure of D_3GV-PDA material post-AC electric field modulation. Hyperspectral images of each condition after being mounted on a cover slide. (a) Brightfield images of (i) self-assembled peptide-DAs, (ii) 10 min UV exposure, (iii) 10 min UV + 30 min DEP and (iv) 30 min DEP + 10 min UV at 50× magnification (500 μm scale bar). The self-assembled D_3GV-DA was shown as a visual reference for the baseline structure of the supramolecular assembly under pH ~5, prior to photopolymerization. Using reference spectral profiles from the (b) 10 min UV sample at pH 5 (yellow) and (c) 10 min UV sample at pH 10 sample (red), SAM was conducted for conditions (ii) to (iv).

the majority chromatic phase domain present in discrete 1-D PDA structures in DEP-exposed samples. While there are local regions that seem to have an increase in red-phase domains (*i.e.*, blue-like to red spectral ratio in Figure 4a SAMs for (ii), (iii), and (iv) are 2.5, 1.2, and 0.7, respectively), multiple regions show very minimal red-phase domain spectral signature (Figure S10; blue-like to red spectral ratios ranging from ~28 to ~78). These data show that conformational heterogeneity within PDA chains/aggregates is not dramatically altered by DEP forces, thus resulting in conserved spectral profiles that predominate in discrete peptide-PDA aggregates for both DEP-exposed and control samples.

Lastly, we investigated the capability of LiDEP to manipulate charged D_3GV-DA aggregates under a variety of virtual electrode geometries (Figure 5; Supplementary Videos S5–S6). While the previous sections focused on the influence of DEP forces on the assembly order, polymerization, morphology, and conformation/chromatic phase of peptide-PDAs, this final section evaluates the responsiveness of peptide-DA aggregates to the LiDEP-generated virtual electrodes. Figure 5 shows a time progression of D_3GV-DA aggregation within the virtual electrodes projected onto the photoconductive surface of the LiDEP chip. Upon the initial application of the AC electric field, a spontaneous clustering of larger aggregates and the accumulation of smaller aggregates over time was observed. Within the 3-minute exposure window, we were able to visualize the DEP-induced migration of the material towards the center of the virtual electrodes, as well as a higher concentration of aggregates within this region. The light-exposed region shows a change in color, indicative of peptide-DA photopolymerization. Since we are working in a non-viscous media where diffusion in and out of the virtual electrode region can easily occur, and AC electric field could also have an inherent effect on the polymerization of peptide-DAs, a subtle color switch was observed even outside of the electrodes. There is also an apparent decrease in positive DEP response when using LiDEP under the same conditions as the quadrupole device (10 kHz and 20 V_{pp}). We attribute this observation to the nature of the experimental setup that relies on a diffuse projector light source, in which DEP force and electric field strength are directly influenced by light intensity and electrode resolution.[39,40] Furthermore, we observed some stochastic directionality in the motion of materials within the channel once the electric field is applied, which is not uncommon when working with nanostructures, due to the increased effect of Brownian motion and hydrodynamics as structures approach the nanometer dimension.[41,42] This describes some random movement of the polymeric aggregates upon DEP field stimulation, as well as the slight unidirectional flow of material initially present within the device. We also note some observed interactions of the aggregates at the virtual electrode boundaries (causing perpendicular alignment) that can be due to electric field gradients. Therefore, we take into account the response of the D_3GV-DA aggregates as they go into the light projection before deviating mildly toward the electrode boundary. From these observations, in conjunction with measurements in prior sections, we show that DEP-based manipulation techniques could be applied as a method to manipulate and fabricate supramolecular aggregates with minimal perturbations on the preset or peptide-templated local structural features under the identified conditions, particularly once the covalent linkages are already formed. Further optimization of the LiDEP manipulation approach shown here can open the avenue to generate micropatterns from supramolecular assemblies, as well as the potential to generate polymorphic micropatterns from supramolecular aggregates of DA material, which can be beneficial for cell scaffolding studies.

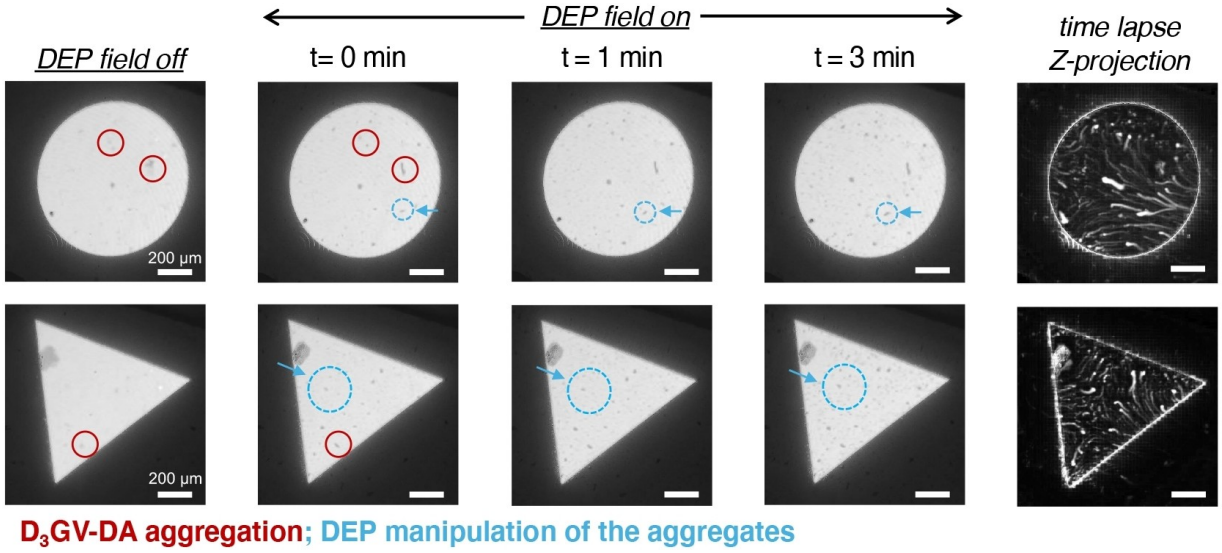

Figure 5. Time progression of D_3GV-DA aggregate manipulation via LiDEP device. Spontaneous aggregation of D_3GV-DA within the device (red). Over a three-minute time frame, we observed the collection of DEP-responsive D_3GV-DA aggregates into the virtual electrodes (blue). Z-projections from collated time-lapse images show the bulk movement of material with respect to the projected virtual electrode.

Conclusions

In summary, we investigated the impact of non-uniform electric fields (*i.e.*, DEP stimuli) on the supramolecular assembly and polymeric aggregates of an amphiphilic peptide-DA conjugate system. We reveal the length scales by which the polymer structure is conserved or influenced by DEP forces. Specifically, subtle changes in chain conformation-dependent blue vs. red chromatic phase ratio can be observed if supramolecular assemblies of peptide-DAs were exposed to DEP forces, but not when the DEP forces were applied post-photopolymerization. While non-uniform AC electric fields are capable of having subtle impacts on supramolecular assembly order, our results show that the chain conformation-dependent chromatic phases adapted by UV-polymerized PDAs tends to be conserved no matter how long the DEP exposure is. Despite the apparent aggregation of peptides on the quadrupole electrodes, we see the conservation of assembly chirality and 1-D morphologies as observed from CD spectra and AFM/TEM images, which can be attributed to the charged nature of D_3GV-DA/PDA resisting crowding-induced lateral bundling of the 1-D structures. Heterogeneity within the 1-D structures studied via hyperspectral microscopy also supports that the predominant chromatic phase domains are maintained even after exposure to DEP. Finally, using a LiDEP platform, we showed that the D_3GV-DA supramolecular aggregates can be manipulated in response to virtual electrodes. Collectively, our findings enable a better understanding of how DEP forces can be used to fine-tune the structure-dependent functionality of a chromogenic polymer such as PDA, as well as the conditions that allow for the conservation of structural features during DEP manipulation of the supramolecular aggregates. These insights offer pathways in the future for fabricating micropatterned supramolecular-based materials with minimal or fine-tunable impact on the assembly to chain-level structural features preset by the molecular design of their building blocks, which is critical for macromolecular systems whose hierarchical structure directly impacts its material function.

Author Contributions

The authors listed above have all substantially contributed to this work and have approved the final version of the manuscript.

Acknowledgements

This work was partially supported by the National Science Foundation (DMR-2239647) and the University of California, Irvine (UCI). K. L. L. is supported by the National Heart, Lung, and Blood Institute (NHLBI) of the National Institutes of Health (NIH) under supplement award number R01HL164348-01A1S1. The authors acknowledge the use of facilities and instrumentation at the UC Irvine Materials Research Institute (IMRI), which is supported in part by the National Science Foundation through the UCI Materials Research Science and Engineering Center (DMR-2011967). We thank Mo Kebaili from the Integrated Nanosystems Research Facility (INRF) Facility at UC Irvine for the fabrication of the photoconductive material for the LiDEP devices. We acknowledge Dr. Xuekun Lu for the fabrication of the quadrupole electrodes at the San Diego Nanotechnology Infrastructure (SDNI) of UC San Diego, a member of the National Nanotechnology Coordinated Infrastructure, which is supported by the National Science Foundation (ECCS-2025752). We also thank Lexi Crowell-Simpkins for her assistance with the preliminary characterization of peptide-DA using DEP, Caleb Chung for his contribution to peptide synthesis, Dr. Dmitri Cordova for his contribution and assistance with the SAM processing, as well as Dr. Dmitry Fishman for the access to CD equipment in the Laser Spectroscopy Laboratories at UC Irvine. Lastly, we would like to thank James Cho from the NSF BioPACIFIC MIP at the California NanoSystems Institute at the University of California, Los Angeles for providing advice on TEM sample preparation procedure.

Conflict of Interests

The authors declare that the research was conducted in the absence of any commercial or financial relationships that could be construed as a potential conflict of interest.

Data Availability Statement

The data that support the findings of this study are available from the corresponding author upon reasonable request.

Keywords: Supramolecular assembly · Peptide-polymer conjugates · Dielectrophoresis · Aggregates · External electric field

[1] A. Ghosh, M. Haverick, K. Stump, X. Yang, M. F. Tweedle, J. E. Goldberger, *J. Am. Chem. Soc.* **2012**, *134*, 3647–3650.
[2] Y. Chen, H. X. Gan, Y. W. Tong, *Macromolecules* **2015**, *48*, 2647–2653.
[3] S. Roy, R. K. Kashyap, P. P. Pillai, *J. Phys. Chem. C* **2023**, *127*, 10355–10365.
[4] Y. Wang, W. Qi, R. Huang, X. Yang, M. Wang, R. Su, Z. He, *J. Am. Chem. Soc.* **2015**, *137*, 7869–7880.
[5] R. A. Nallicheri, M. F. Rubner, *Macromolecules* **1991**, *24*, 517–525.
[6] R. Klajn, K. J. M. Bishop, B. A. Grzybowski, *Proc. Nat. Acad. Sci.* **2007**, *104*, 10305–10309
[7] S. Sun, H.-W. Liang, H. Wang, Q. Zou, *ACS Nano* **2022**, *16*, 18978–18989.
[8] A. F. Demirörs, P. P. Pillai, B. Kowalczyk, B. A. Grzybowski, *Nature* **2013**, *503*, 99–103.
[9] L. Sardone, V. Palermo, E. Devaux, D. Credgington, M. d. Loos, G. Marletta, F. Cacialli, J. v. Esch, P. Samorì, *Adv. Mater.* **2006**, *18*, 1276–1280.
[10] B. A. Grzybowski, C. E. Wilmer, J. Kim, K. P. Browne, K. J. M. Bishop, *Soft Matter* **2009**, *5*, 1110.
[11] C. M. Kelly, T. Northey, K. Ryan, B. R. Brooks, A. L. Kholkin, B. J. Rodriguez, N.-V. Buchete, *Biophys. Chem.* **2015**, *196*, 16–24.
[12] F. P. Cometto, N. Arisnabarreta, R. Vanta, D. K. Jacquelín, V. Vyas, B. V. Lotsch, P. A. Paredes-Olivera, E. M. Patrito, M. Lingenfelder, *ACS Nano* **2024**, *18*, 4287–4296.
[13] S. Kumar, P. J. Hesketh, *Nanotechnology* **2010**, *21*, 325501.

[14] T. L. Morkved, M. Lu, A. M. Urbas, E. E. Ehrichs, H. M. Jaeger, P. Mansky, T. P. Russell, *Science* **1996**, *273*, 931.
[15] T. B. Jones, *IEEE Eng. Med. Biol. Mag.* **2003**, *22*, 33–42.
[16] A. S. Mohamad, R. Hamzah, K. F. Hoettges, M. P. Hughes, *AIP Adv.* **2017**, *7*, 015202.
[17] M. Heyden, D. V. Matyushov, *J. Phys. Chem. B* **2020**, *124*, 11634.
[18] T. N. G. Adams, P. A. Turner, A. V. Janorkar, F. Zhao, A. R. Minerick, *Biomicrofluidics* **2014**, *8*, 054109.
[19] K. L. Lacy, S. Salib, M. Tran, T. Tsai, R. Valentine, H. A. M. Ardoña, T. N. G. Adams, *J. Visualized Exp.* **2023**, *196*, e64909.
[20] T. Tsai, P. D. Vyas, L. L. Crowell, M. Tran, D. W. Ward, Y. Qin, A. Castro, T. N. G. Adams, *Electrophoresis* **2024**, *45*, 1–12.
[21] C. L. Asbury, A. H. Diercks, G. van den Engh, *Electrophoresis* **2002**, *23*, 2658–2666.
[22] M. Hoeb, J. O. Rädler, S. Klein, M. Stutzmann, M. S. Brandt, *Biophys. J.* **2007**, *93*, 1032–1038.
[23] J. Huo, Z. Hu, G. He, X. Hong, Z. Yang, S. Luo, X. Ye, Y. Li, Y. Zhang, M. Zhang, H. Chen, T. Fan, Y. Zhang, B. Xiong, Z. Wang, Z. Zhu, D. Chen, *Appl. Surf. Sci.* **2017**, *423*, 951–956.
[24] S. Lim, D. L. M. Cordova, A. S. Robang, Y. Kuang, K. S. Ogura, A. K. Paravastu, M. Q. Arguilla, H. A. M. Ardoña, *Biomacromolecules* **2023**, *24*, 4051–4063.
[25] M. Weston, A. D. Tjandra, R. Chandrawati, *Polym. Chem.* **2020**, *11*, 166–183.
[26] J. P. Yapor, A. Alharby, C. Gentry-Weeks, M. M. Reynolds, A. K. M. M. Alam, Y. V. Li, *ACS Omega* **2017**, *2*, 7334.
[27] J. Song, Q. Cheng, S. Kopta, R. C. Stevens, *J. Am. Chem. Soc.* **2001**, *123*, 3205–3213.
[28] J. P. Lee, H. Hwang, S. Chae, J.-M. Kim, *Chem. Commun.* **2019**, *55*, 9395–9398.
[29] L. Luo, C. Wilhelm, A. Sun, C. P. Grey, J. W. Lauher, N. S. Goroff, *J. Am. Chem. Soc.* **2008**, *130*, 7702–7709.
[30] J. T. Wen, J. M. Roper, H. Tsutsui, *Ind. Eng. Chem. Res.* **2018**, *57*, 9037–9053.
[31] Y. Kuang, Z.-F. Yao, S. Lim, C. Ngo, M. A. Rocha, D. A. Fishman, H. A. M. Ardoña, *Macromolecules* **2023**, *56*, 4526–4540.
[32] T. R. Sudarshan, S. Lim, J. Li, A. S. Robang, L. M. Liberty, H. A. M. Ardoña, A. K. Paravastu, *Solid State Nucl. Magn. Reson.* **2024**, *133*, 101959.
[33] J. Schindelin, I. Arganda-Carreras, E. Frise, V. Kaynig, M. Longair, T. Pietzsch, S. Preibisch, C. Rueden, S. Saalfeld, B. Schmid, J.-Y. Tinevez, D. J. White, V. Hartenstein, K. Eliceiri, P. Tomancak, A. Cardona, *Nat. Methods* **2012**, *9*, 676–682.
[34] Y.-W. Lu, C. Sun, Y.-C. Kao, C.-L. Hung, J.-Y. Juang, *Nanomaterials (Basel)* **2020**, *10*, 1364.
[35] R. D. Miller, T. B. Jones, *Biophys. J.* **1993**, *64*, 1588–1595.
[36] B. Çetin, D. Li, *Electrophoresis* **2011**, *32*, 2410–2427.
[37] X. Sun, T. Chen, S. Huang, L. Li, H. Peng, *Chem. Soc. Rev.* **2010**, *39*, 4244.
[38] J. Chen, J. Zheng, Y. Hou, K. Sugihara, *Chem. Commun.* **2023**, *59*, 3743–3746.
[39] W. Choi, S.-W. Nam, H. Hwang, S. Park, J.-K. Park, *Appl. Phys. Lett.* **2008**, *93*, 143901.
[40] D. Keck, S. Ravi, S. Yadav, R. Martinez-Duarte, *Micromachines (Basel)* **2024**, *15*, 342.
[41] M. Washizu, S. Suzuki, O. Kurosawa, T. Nishizaka, T. Shinohara, *IEEE Trans. Ind. Appl.* **1994**, *30*, 835–843.
[42] A. Nakano, A. Ros, *Electrophoresis* **2013**, *34*, 1085–1096.

Manuscript received: July 31, 2024
Accepted manuscript online: October 9, 2024
Version of record online: ■■, ■■